Aerodynamics of Two-Dimensional Blade-Vortex Interaction

G. R. Srinivasan*
JAI Associates, Inc., Mountain View, California
and
W. J. McCroskey† and J. D. Baeder‡
U.S. Army Aeroflightdynamics Directorate—AVSCOM
NASA Ames Research Center, Moffett Field, California

Unsteady interaction of a helicopter rotor blade with a passing vortex is numerically calculated using the two-dimensional, thin-layer Navier-Stokes equations and a prescribed vortex approach at subsonic and transonic flow conditions. The results are compared with the recent experimental data of Caradonna et al. for a two-bladed rotor in forward flight. The comparisons show that, for the subcritical flow case, the unsteady lag effects on the basic rotor blade are absent and the three-dimensional effects appear to be negligible. The numerical results are in good agreement with the experimental data. At the supercritical flow condition, however, the flowfield is dominated by the presence of the shock waves, with strong indications of unsteady time lags in the shock-wave motions and strengths and of important three-dimensional effects, even in the absence of the vortex interaction. Hence, for this case, the two-dimensional calculations fail to predict the basic rotor flowfield. The presence of strong three-dimensional influence in the supercritical flow data is demonstrated through transonic small-disturbance calculations, whereas similar calculations for the subcritical flow condition showed almost no three-dimensional influence. Finally, the details of the experimental vortex structure were found to be important in matching the numerical results with the experimental data.

Nomenclature

A, B, C_1, C_2, D, E = coefficients, see Eq. (10)
$\hat{A}, \hat{B}$ = Jacobian matrices
a_0 = vortex core radius
a_∞ = freestream sound speed
C = characteristic length scale, chord of the rotor blade
C_L = lift coefficient
C_M = quarter-chord pitching-moment coefficient
C_p = pressure coefficient
C_w = chord of the vortex-generating wing
$\hat{E}, \hat{E}_0$ = flux vectors
e = total energy per unit volume
$\hat{F}, \hat{F}_0$ = flux vectors
I = identity matrix
J = transformation Jacobian
$\hat{M}$ = Jacobian matrix of viscous stress flux vector
M_ℓ = local Mach number
M_r = blade reference Mach number, $= \Omega r_B a_\infty$
M_T = blade tip Mach number
M_∞ = freestream Mach number
p = static pressure
$\boldsymbol{Q}$ = velocity induced by the vortex, $= iu_v + jv_v$
$\hat{q}$ = unknown flowfield vector
$\hat{q}_0$ = Euler solution of vortex in a uniform freestream
R = radius of rotor blade
Re = Reynolds number
r = radial distance from the vortex center
r_B = reference station on the rotor blade
r_0 = initial vortex position, $= ix_0 + jy_0$
r_w = r/C_w
$\hat{S}$ = viscous flux vector
t = time
U, V = contravariant velocity components
U_∞ = forward velocity of rotor or tunnel velocity
u, v = velocity components in physical plane
u_v, v_v = velocity components induced by the vortex
v_θ = tangential velocity of vortex
x_v, y_v = instantaneous vortex position
x, y, z, t = physical plane coordinates
y_b = airfoil surface, $= y_b(x, t)$
α = angle of attack
Γ = vortex strength
$\hat{\Gamma}$ = dimensionless strength of vortex, $= \Gamma/M_r a_\infty C$ or $\Gamma/M_\infty a_\infty C$
γ = ratio of specific heats
δ = airfoil thickness ratio
ϵ = inverse of blade aspect ratio, $= C/R$
ϵ_E, ϵ_I = explicit and implicit smoothing coefficients, respectively
θ = angle between the vortex velocity vector and y axis
Λ = angle between vortex axis and rotor-blade chord line
μ = advance ratio, $= U_\infty/\Omega R$
μ' = local advance ratio, $= U_\infty/\Omega r_B$
$\xi_x, \xi_y, \ldots$ = metrics of transformation
ξ, η, τ = transformed plane coordinates

Presented as Paper 85-1560 at the AIAA 18th Fluid Dynamics, Plasmadynamics and Lasers Conference, July 16-18, 1985; received Aug. 9, 1985; revision received Jan. 20, 1986.

*Senior Research Scientist. Member AIAA.
†Senior Staff Scientist. Associate Fellow AIAA.
‡Research Scientist. Member AIAA.

ρ = density
Φ = disturbance potential
ψ = azimuth angle (Fig. 2)
Ω = angular velocity of the rotor blade

Introduction

ONE important problem of helicopter aerodynamics that has been the subject of many recent experimental[1-4] and theoretical[5-11] studies is the mechanism of blade-vortex interaction. This interaction mechanism is a primary source of impulsive noise generation. The transonic speeds of today's helicopter blade tips add to the complexity of the problem. The blade tips, which trail the strong and concentrated tip vortices in such a flowfield, trace out prolate cycloidal paths in space, and, in the process, encounter a variety of blade-vortex interactions. These interactions induce unsteady blade loading and aerodynamic noise, with compressibility playing an important role in the problem.

The generic problem of the blade-vortex interaction can be viewed, in general, as unsteady and three-dimensional; however, in one limit, when the intersection angle of the vortex with the blade (Λ) is very small or zero, the interaction can be approximated to be two-dimensional but unsteady, (see Fig. 1). Most of the recent numerical studies[5-11] that have addressed this problem have been solved in this limit. Transonic small-disturbance equations,[5-9] full-potential equations,[11] Euler equations,[7-10] and thin-layer Navier-Stokes equations[7-9] all have been solved for the problem of a convecting vortex passing and interacting with the flowfield of a stationary airfoil in a uniform freestream.

Some of the preceding methods place limitations on the intensity of the interaction in terms of vortex strength, vortex location with respect to the airfoil, and on the freestream Mach number; nevertheless, they all seem to give similar results. For flows dominated by the strong viscous interaction and shock-wave/boundary-layer interaction, the natural choice of the equation set that describes such a flow completely would be the Navier-Stokes equations. Present-day numerical algorithms for this set of equations are still very expensive in terms of computing time, although much progress has been made toward reducing the time required. However, the memory of the available computers is adequate to address these types of problems in the two-dimensional limit. This is particularly true with the present prescribed-vortex, or perturbation, method which has been demonstrated to resolve important flow features in a blade-vortex interaction problem in both subsonic and transonic flows, even in a very sparse finite difference mesh.[7-9]

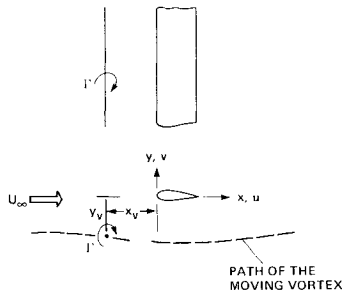

Fig. 1 Schematic of parallel blade-vortex interaction, in the limit of $\Lambda = 0$, and definition of coordinate system.

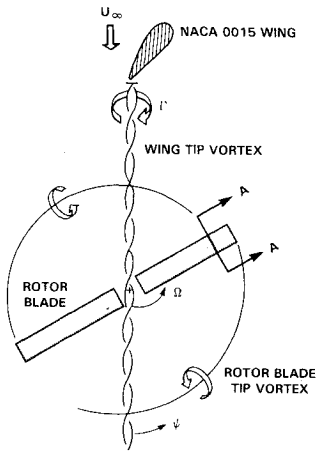

Fig. 2 Schematic of experimental model rotor tests of Ref. 1.

A problem more practical and numerically more complicated than the one mentioned previously is that of a rotating blade of a helicopter rotor encountering a vortex generated upstream. Such an experiment was done recently in a wind tunnel at the U.S. Army Aeromechanics Laboratory (presently called Aeroflightdynamics Directorate, U.S. Army Aviation Research and Technology Activity—AVSCOM) at NASA Ames Research Center.[1] A schematic of the experiment is shown in Fig. 2. A vortex generated at the tip of a straight NACA-0015 wing interacts with the flowfield of a rotating, two-bladed helicopter rotor blade under subsonic and transonic flow conditions. For such a rotating blade, unlike the stationary airfoils considered in previous studies,[5-11] the unsteady time-lag effects that are present even in the absence of the interacting vortex are very important.[12] The effect of this unsteady time lag is to delay the process of flow adjustment corresponding to the appropriate azimuthal blade position. This has a profound influence on the unsteady blade loads at transonic conditions. In addition, the results may also be influenced by the three-dimensional (tip) effects, if the chordwise reference station considered is closer to the blade tip. Another very important ingredient of the vortex interaction study is the detailed knowledge of the structure of the interacting vortex. Although an analytical representation of the vortex is often used, the point to bear in mind is that such a representation should have an accurate core structure embedded in it.

In the present investigation, it was found that the rotor-blade reference station of Ref. 1 (section AA in Fig. 2) that undergoes parallel blade-vortex interaction is inboard of the blade tip region. If the tip influence is neglected at this station, the flow can be approximated as two-dimensional, but unsteady. One important difference of this problem from the earlier formulation[7-9] is that the blade is rotating now. After implementing this important feature, along with the necessary changes in the boundary conditions, unsteady, two-dimensional, thin-layer Navier-Stokes equations in strong conservation-law form are solved for the interaction flowfield of the rotating blade using an approximately factored, implicit, finite difference numerical algorithm written in delta form.[7-9,13] An analytical representation of the measured vortex structure was used in the computations.

Although the initial finite difference grids were generated by an algebraic method,[14] an adaptive-grid procedure[15,16] was used throughout to resolve the important flow features, including shock waves, vortex/shock-induced separation of the boundary layers, if any, and the vortex structure itself.

In this paper, the governing equations and numerical formulations are discussed, and the numerical results and comparisons with experimental data are presented.

Governing Equations and Solution Procedure

The interaction flowfield is solved by the prescribed-vortex, or perturbation, method.[17] The essence of the method is that each of the dependent flow variables is split into a prescribed part, which is simply the vortical disturbance, and a remaining part, which is obtained from the solution of the governing

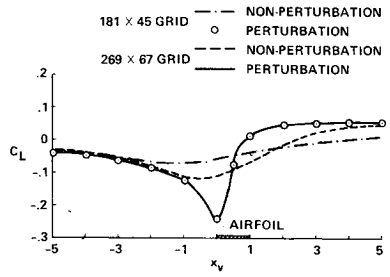

Fig. 3 Effectiveness of the prescribed-vortex method compared with the nonperturbation method. Euler results for airfoil-vortex interaction: NACA 64A006 airfoil, $M_\infty = 0.85$, $\alpha = 0$ deg, $\hat{\Gamma} = 0.2$, $a_0 = 0.05$, and $y_0 = y_v = -0.26$.

equation set. Even though the governing equations are nonlinear and independent solutions are not superposable, the dependent variables can still be decomposed as

$$q = q_0 + (q - q_0)$$

where

$$q = \begin{bmatrix} \rho \\ \rho u \\ \rho v \\ e \end{bmatrix} \quad \text{and} \quad q_0 = \begin{bmatrix} \rho \\ \rho u \\ \rho v \\ e \end{bmatrix}_v \tag{1}$$

Here q is the unknown flowfield vector, and the vector q_0 represents the solution of Euler equations for the vortical disturbance convecting in a uniform freestream. Previous studies[7-9] have demonstrated that the perturbation method can, in fact, resolve the flows with concentrated vortices well, even with a coarser grid when compared to a nonperturbation method.[18] For example, a representative plot of the variation of lift coefficient as a function of the vortex position is reproduced from Ref. 8 in Fig. 3. This calculation was done using Euler equations for the case of a convecting vortex encountering a nonlifting, stationary NACA-64A006 airfoil in transonic flow, and using the same grid topology with both perturbation and nonperturbation (or conventional) methods. This figure clearly demonstrates that with the conventional method the accuracy of the solution increases with the fineness of the finite difference mesh, whereas the perturbation method produces a much better solution even in a coarser mesh.

The governing partial differential equations are the unsteady, thin-layer Navier-Stokes equations.[19] The equations are written in nondimensional, strong conservation-law form for a perfect gas using the generalized independent coordinate system of

$$\xi = \xi(x, y, t), \qquad \eta = \eta(x, y, t), \qquad \tau = \tau(t) \tag{2}$$

and in the perturbation form[7-9] as

$$\partial_\tau(\hat{q} - \hat{q}_0) + \partial_\xi(\hat{E} - \hat{E}_0) + \partial_\eta(\hat{F} - \hat{F}_0) = Re^{-1}\,\partial_\eta \hat{S} \tag{3}$$

where $\hat{(\ )}$ denotes quantities scaled by the Jacobian, e.g.,

$$\hat{q} = J^{-1}q; \quad \hat{q}_0 = J^{-1}q_0 \tag{4}$$

and

$$J = \xi_x\eta_y - \xi_y\eta_x = 1/(x_\xi y_\eta - x_\eta y_\xi)$$

is the transformation Jacobian. The flux vectors $\hat{E}$, $\hat{E}_0$, $\hat{F}$, $\hat{F}_0$, and $\hat{S}$ are described in detail in Refs. 7-9. The viscous flux vector $\hat{S}$ is written in the context of a thin-layer model[19] and, hence, is valid for high-Reynolds-number turbulent flows. The turbulent eddy viscosity is computed using a two-layer, algebraic eddy-viscosity model.[20]

The generalized coordinate system of ξ, η, τ allows the boundary surfaces in the physical plane to be mapped onto rectangular surfaces in the computational plane. This feature simplifies the procedure of grid-point clustering in the flow regions that experience rapid change in the flowfield gradients.

The primitive variables that make up the governing equations, Eq. (3), are density ρ, the two mass fluxes ρu and ρv in the two coordinate directions x and y (where x is the streamwise direction and y is normal to it), and the total energy per unit volume, e. All length scales are normalized by the chord of the rotor blade at the reference station, and the dependent variables ρ, p, e, u, and v by ρ_∞, γp_∞, $\rho_\infty a_\infty^2$, and a_∞, respectively.

The pressure, density, and velocity components are related to the energy per unit volume by the equation of state, which is written for a perfect gas as

$$e = \frac{p}{\gamma - 1} + \rho\left(\frac{u^2 + v^2}{2}\right) \tag{5}$$

This equation of state, along with the mass and momentum equations given by Eq. (3), completes the equation set to be solved.

In the present formulation, the difference between the problems of the stationary and moving blades shows up in the metric terms involving time derivatives, namely, ξ_t and η_t. Following the formulation given by Isom[21] and Caradonna and Isom[22] for unsteady flow over helicopter rotor blades, the effective local Mach number at the reference station can be written as

$$M_\ell = M_r(1 + \mu' \sin\Omega t) \tag{6}$$

where M_r is the rotational Mach number, μ' the local advance ratio, and Ω the angular velocity of the rotating blade. This formulation enables the flowfield solution of a rotating blade with an oncoming freestream to be solved in the two-dimensional limit as a blade moving with an x velocity of $M_r a_\infty \mu' \sin\Omega t$ in a flow of Mach number M_r. Note that both ξ_t and η_t are nonzero for this case, whereas, for a stationary blade with a fixed grid, both ξ_t and η_t are zero.

The boundary conditions are applied explicitly. Since the grid extends 20 chord lengths in all directions from the surface of the blade, freestream conditions are specified at the outer boundary and simple extrapolation is used for ρ, ρu, and ρv at the outflow boundary. For supersonic flow, the total energy e is also extrapolated; but for subsonic flow, the pressure is held constant at the freestream value, and e is obtained from Eq. (5). To ensure continuity across the wake cut, the flow variables are linearly extrapolated to obtain the values along the cut.

Along the body surface $\eta(x, y, t) = 0$, the no-slip condition for viscous flow without suction or injection is given by setting U and $V = 0$. The pressure along the body surface is obtained by solving the normal momentum equation, and the density at the surface is obtained by extrapolation from the grid interior. The total energy e is calculated from the known pressure and density at the surface. The boundary conditions are of low order and, hence, require that the grid be clustered and normal at the body surface.

The interacting vortex is initialized at an upstream location of the airfoil, typically at or near the upstream grid boundary as in Ref. 9. The vortex flow vector $\hat{q}_0$ is determined as follows. The cylindrical velocity is analytically prescribed either by a Lamb-like distribution or by fitting a smooth curve through the experimental data, if available. For this vortex convecting in a uniform freestream, the induced pressure and density fields are determined numerically by solving the radial momentum equation in conjunction with the energy equation for constant enthalpy flow. With the velocity, density, and

pressure fields known, the total energy e_v is determined from the energy equation.

Surface conforming grids are needed to simplify the application of the body-boundary condition procedure. In this study, an adaptive gridding procedure of Nakahashi and Deiwert[15,16] is used to resolve flow features and to improve the accuracy of the numerical method. Briefly, the method uses tension and torsion spring analogies. The tension spring, which connects the adjacent grid points to each other, controls grid spacings so that clustering is obtained in regions containing shock waves and shear layers. On the other hand, the torsion spring, which is attached to each grid node, controls inclinations (angles) of coordinate lines and prevents excessive grid skewness. The mesh can be made nearly orthogonal at the surface. A marching procedure is used that results in a simple tridiagonal system of equations at each coordinate line to determine the grid-point distribution. Multidirectional grid adaptation is achieved by successive application in each direction. For the compressible flowfields considered in this study, the density gradient was found to be the best choice to drive the adaption in the x direction; the Mach number gradient was the best choice of driver in the normal direction. In actual practice, for a given baseline grid, the preceding procedure will modify the grid at specified intervals to resolve the flow satisfactorily. In the present study, the grid was adapted at every two marching steps interval. This increased the computational time by approximately 50%. The baseline grid used was a surface-conforming C-grid generated by an algebraic method of Pulliam et al.[14] and had 221 points around the airfoil and 67 points in the normal direction. The grid boundary was chosen to be at 20 chords in all directions.

An implicit, spatially factored numerical algorithm with Euler-implicit time differencing[13] is used to solve the perturbation form of Eq. (3). This algorithm is written in delta form as

$$\begin{aligned}&\left(I+h\delta_\xi\hat{A}^n-\epsilon_I J^{-1}\nabla_\xi\Delta_\xi J\right)\\&\times\left(I+h\delta_\eta\hat{B}^n+h\delta_\eta\hat{M}^n-\epsilon_I J^{-1}\nabla_\eta\Delta_\eta J\right)\left(\Delta\hat{q}^n-\Delta\hat{q}_0^n\right)\\&=-\Delta t\left[\delta_\xi\left(\hat{E}^n-\hat{E}_0^n\right)+\delta_\eta\left(\hat{F}^n-\hat{F}_0^n\right)-Re^{-1}\delta_\eta\hat{S}^n\right]\\&-\epsilon_E J^{-1}\left[\left(\nabla_\xi\Delta_\xi\right)^2+\left(\nabla_\eta\Delta_\eta\right)^2\right]J\left(\hat{q}^n-\hat{q}_0^n\right)\end{aligned}\tag{7}$$

where $\hat{A}$, $\hat{B}$, and $\hat{M}$ are the Jacobian matrices detailed in Ref. 19, I the identity matrix, δ_ξ and δ_η the spatial central difference operators, and Δ and ∇ the forward and backward difference operators, respectively. For convenience, $\Delta\xi = 1 = \Delta\eta$ is assumed. The time index is denoted by h, and $\hat{q}^n = \hat{q}^n(n\Delta t)$, $\Delta\hat{q}^n = \hat{q}^{n+1} - \hat{q}^n$, and ϵ_I and ϵ_E are the implicit and explicit smoothing coefficients, respectively. Second-order implicit and fourth-order explicit numerical dissipation terms are added to the numerical scheme to improve the nonlinear stability limits posed by the fine mesh.[23] Even so, the nondimensional time steps generally were restricted by the stability constraints to the order of 0.05 deg of the azimuthal travel of the blade motion or 0.005455 of the chord travel.

The numerical scheme is first-order accurate in time and second-order accurate in space. Further, in writing Eq. (7), it is assumed that $\hat{A}_0 \cong \hat{A}$ and $\hat{B}_0 \cong \hat{B}$, where $\hat{A}_0 = \partial\hat{E}_0/\partial\hat{q}_0$ and $\hat{B}_0 = \partial\hat{F}_0/\partial\hat{q}_0$.

Central differencing is used throughout the solution domain, except in regions of supersonic flow before shock waves, where upwind differencing is used. The transformation metrics are not known analytically and are computed numerically by central differencing (second order) at the interior points and by three-point, one-sided differencing at the boundaries.

Results for a Stationary Rotor Airfoil

In this section, numerical results are presented for a moving vortex encountering a fixed rotor blade under transonic conditions. All calculations are done for an NACA-0012 airfoil in a uniform freestream of $M_\infty = 0.8$ at $\alpha = 0$ deg, and assuming a turbulent boundary layer. As mentioned previously, an adaptive gridding procedure is used in all of the results presented here.

A Lamb-like vortex with a finite viscous core ($a_0 = 0.05$) and a cylindrical velocity distribution given by[7-9]

$$\frac{v_\theta(r)}{a_\infty} = \frac{\hat{\Gamma}}{2\pi r}M_\infty\left(1-e^{-r^2/a_0^2}\right)\tag{8}$$

was chosen to interact with the flowfield of a stationary, nonlifting rotor airfoil in a uniform freestream of Mach number M_∞. The strength of the vortex and its location with respect to the airfoil were chosen to be $\hat{\Gamma} = 0.2$ and $y_v = -0.26$, respectively. The interaction flowfield was computed in the same manner as outlined in earlier studies.[7-9] Figure 4 shows plots of instantaneous surface-pressure distributions, the local grid arrangement, and the Mach number contours for different x locations of vortex positions as the vortex passes by the airfoil. The passing vortex induces on the airfoil a continually changing effective angle of attack. Because of the sense of rotation, it induces a downwash initially when it is upstream of the leading edge, changing to upwash as it passes behind the airfoil. This induces a continuous change in the blade-loading pattern. It should be noted here that the initial lift on the blade is zero and that any lift generated during the interaction is induced solely by the vortex. As observed previously,[7-9] the maximum influence of the vortex on the airfoil flowfield seems to occur when the vortex is within one chord of the airfoil.

Previous calculations done for the same airfoil under identical conditions[24] used a fixed-grid topology, with 221×67 grid points; in that study, the shocks were not well resolved. In the present case, the adaptive-grid topology, shown in Fig. 4, also uses 221×67 grid points, but is clearly able to resolve all aspects of the flow. Since the grid is adapted in both the x and y directions, it clearly resolves shock waves, the interacting vortex, and the viscous layer at the body surface. Large-scale vortex and shock-induced boundary-layer separation was not observed, although the formation of a small separation bubble and sufficient thickening of the boundary layer were seen behind the shock wave for conditions when the vortex influence was maximum.

As the vortex passes the airfoil, it encounters the shock wave sitting on the surface. The vortex actually splits the shock wave into a triple shock wave, as is clearly seen from the local grid structure and Mach contours of Fig. 4 for a vortex position past the airfoil midchord. This feature was confirmed by making an independent Euler calculation of the same flow, by using a fixed-grid topology, and by heavily clustering the grid in the region of interest. This apparent unsteady effect seems to fade away as the vortex passes several chords downstream of the airfoil trailing edge. Figure 5 shows a plot of instantaneous lift and pitching-moment coefficients as a function of the x-vortex position during the interaction process. The lift coefficient is initially negative (because of the sense of rotation of the vortex), reaches a negative maximum for a vortex position slightly upstream of the leading edge of the airfoil, increases to a near-zero value at $x_v \cong 0.7C$, and stays near that value for the rest of the interaction period. Pitching-moment changes are maximum when the vortex is within $1C$ of the airfoil.

Results for a Rotating Blade

In this section, computational results are presented corresponding to two experimental conditions of Caradonna et al.[1] One condition each of subcritical and supercritical flows with and without vortex encounter will be discussed. The corresponding tip Mach number of the two cases is 0.6 and 0.8, respectively, with an advance ratio of $\mu = 0.2$ for both.

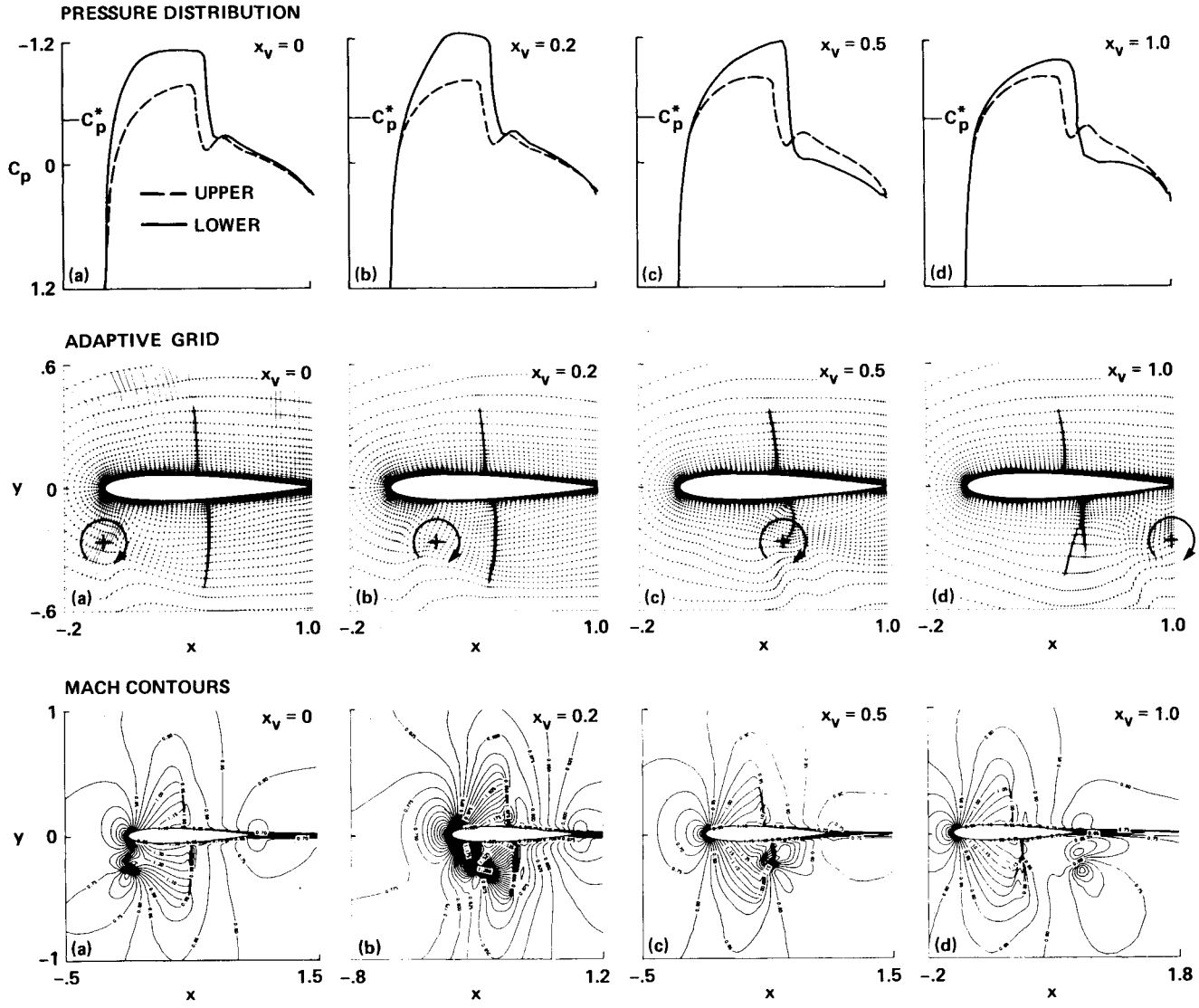

Fig. 4 Instantaneous surface-pressure distributions, adaptive grid, and Mach contours during airfoil-vortex interaction with a convecting vortex: NACA 0012 airfoil, $M_\infty = 0.8$, $\alpha = 0$ deg, $Re = 6 \times 10^6$, $\hat{\Gamma} = 0.2$, $y_0 = y_v = -0.26$. The instantaneous position of the vortex during the interaction is shown on the adaptive grid.

The schematic of the experimental arrangement is shown in Fig. 2. The experiments were performed in a wind tunnel where an NACA-0015 wing generated a tip vortex upstream of a two-bladed, model helicopter rotor. The interacting vortex, of core radius 25 mm, passed the reference rotor spanwise station at $r_B = 0.893$ and at a distance of $y_v = -0.4C$. The chord of the rotor blade was 152.4 mm, and the diameter of the rotor was 2.134 m.

Structure of the Experimental Vortex

Comparison of the numerical results and the experimental data will be meaningful only if the correct structure of the experimental vortex is considered. The strength of the experimental vortex quoted in Ref. 1 is $\hat{\Gamma} = 0.31$ with a core radius of $a_0/C = 0.1667$. Use of these data in Eq. (8) yielded peak velocities some 40% greater than those measured by Takahashi and McAlister[25] and Orloff and Grant[26] for the identical wing under comparable flow conditions, although it had the inviscid vortex, $(1/r)$, behavior well outside the viscous core.

Since the details of the blade-vortex interaction are sensitive to the vortex structure and its peak-induced velocities, the following alternative fit to the experimental data, given by

$$\frac{v_\theta}{\Omega r_B} = \mu' \frac{v_\theta}{U_\infty} = \frac{0.8\hat{\Gamma}}{2\pi r}\left(\frac{r^2}{r^2 + a_0^2}\right) \tag{9}$$

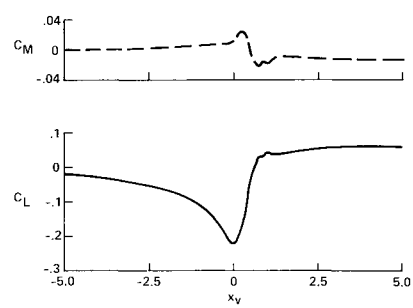

Fig. 5 Lift and pitching-moment variations with instantaneous vortex position for the conditions of Fig. 4.

was used in the numerical calculations. The factor 0.8 was chosen to allow the best match of peak velocity in the available experimental data over the range of angles of attack. Figure 6 shows the resultant agreement with the data[25,26] at the wing incidence used by Caradonna et al.[1] as well as the inviscid behavior.

Subcritical Case

This condition corresponds to $M_T = 0.6$ and $\mu = 0.2$. For the reference station at 89.3% of the rotor blade radius, these conditions translate to $M_r = 0.536$ and $\mu' = 0.223$.

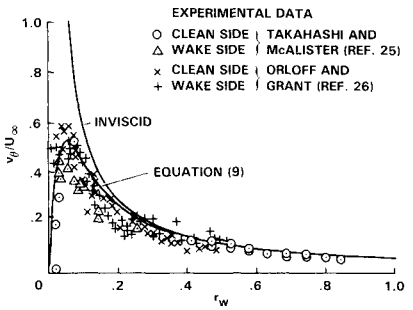

Fig. 6 Tangential velocity distribution of the tip vortex generated by an NACA 0015 wing.

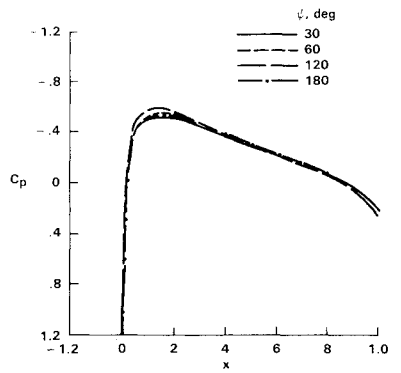

Fig. 7 Instantaneous pressure distributions at the reference blade station for the rotor-alone case: $M_T = 0.6$, $\mu = 0.2$, $r_B = 0.893$.

Results for Rotor Alone

First, consider a nonlifting rotor in forward flight in the absence of vortex interaction. The objective of such an exercise is to determine the importance of three-dimensional, unsteady time-lag effects as the rotor sweeps in azimuth, say, from 0 to 180 deg. As the blade rotates from 0 to 180 deg, its local Mach number increases in the first quadrant, reaching a maximum at the $\psi = 90$ deg position; it again decreases to the average value at $\psi = 180$ deg. In going through this change in local Mach number, if the flow on the rotor at $\psi = 90 + \Delta\psi$ is nearly the same as that at $\psi = 90 - \Delta\psi$, then the rotating blade behaves as if it were quasisteady and quasi-two-dimensional. If, on the other hand, the two flows are different, then the associated three-dimensional or time-lag effects will be expected to have an influence on the vortex-blade interaction flowfield that develops in the vicinity of the $\psi = 180$ deg position.

Figure 7 shows instantaneous surface-pressure results at several azimuth positions of the blade. For this flow, the initial local Mach number for $\psi = 0$ deg is 0.536 and increases to a maximum (based on the local advance ratio) at $\psi = 90$ deg and again decreases to 0.536 at $\psi = 180$ deg. Examination of these pressure distributions indicates that for this subcritical flow condition the unsteady time-lag effects are negligible.

Vortex Encounter with a Rotating Blade

To compute the vortex interaction flowfield, as before, the vortex was initialized at the $\psi = 0$ position of the rotor blade (the corresponding $x_v = -19.638$) as in Refs. 7-9. It then convects with the flow at the effective "freestream velocity," which is $M_r a_\infty (1 + \mu' \sin\psi)$ in this case. Typical instantaneous surface-pressure distributions are shown in Fig. 8 corresponding to several vortex positions as the vortex convects past the rotor blade. Since the rotor is nonlifting, the lift is initially zero, and, as the vortex approaches the blade, it induces a downwash and hence a negative lift. This continuously increases and reverses in sign, becoming positive lift as the

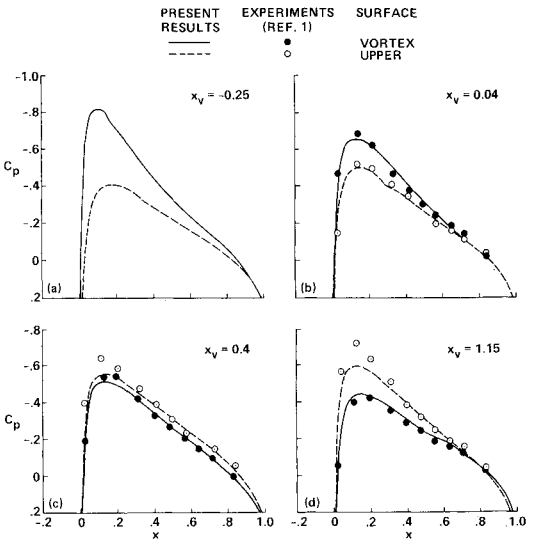

Fig. 8 Instantaneous surface-pressure distributions for the case of blade-vortex interaction: $M_T = 0.6$, $\mu = 0.2$, $r_B = 0.893$, $\hat{\Gamma} = 0.31$, $y_v = -0.4$.

vortex passes the airfoil. Shown in this figure are data from experiments of Caradonna et al.[1] The comparison of numerical results and experimental data shows good agreement, both qualitatively and quantitatively, although the peak pressures on the side of the blade opposite the vortex seem to be underpredicted. It should be pointed out here that, in the experiments, the rotor model had pressure taps on one surface only. To get the pressure distribution on both of the surfaces, the model was simply inverted, and a second, almost identical, experiment was run. Nevertheless, it is gratifying to see such good agreement with experiments. Thus far, three-dimensional effects have been neglected, whose influence at this flow condition appears minimal.

Supercritical Case

This condition corresponds to a tip Mach number of 0.8, with an advance ratio of 0.2, and the blade reference station $r_B = 0.893$, as before. This translates to a reference Mach number of 0.714 and a local advance ratio μ' of 0.223.

Results for Rotor Alone

We first present results for the rotor-alone case (i.e., in the absence of vortex interaction). Figure 9 shows plots of instantaneous surface-pressure distributions at four rotor blade azimuthal positions. As before, the initial lift on the rotor blade (at $\psi = 0$ deg) is zero and the flow is subcritical; as the blade rotates its local effective Mach number increases, reaching a maximum at $\psi = 90$ deg and decreasing in the second quadrant. As seen in these pressure-distribution plots, the shock wave that develops as the blade rotates gets stronger and moves toward the trailing edge of the airfoil. Even though the effective local Mach number reaches a maximum for $\psi = 90$ deg, the shock wave continues to get stronger and move toward the trailing edge in the second quadrant before it begins moving upstream toward the leading edge of the blade. This unsteady time lag in the growth and decay of the shock wave persists even when the rotor blade has passed the 180 deg azimuthal position into the third quadrant.

Comparison of experimental data[27] with numerical results in Fig. 9 shows relatively good agreement concerning the pressure levels for all blade azimuthal positions up to $\psi = 150$ deg, but the location of the shock wave is too far aft in the second quadrant. In the experiments, the shock wave seems to have collapsed between the azimuth positions of $\psi = 150$ and 180 deg. But the numerical results show the

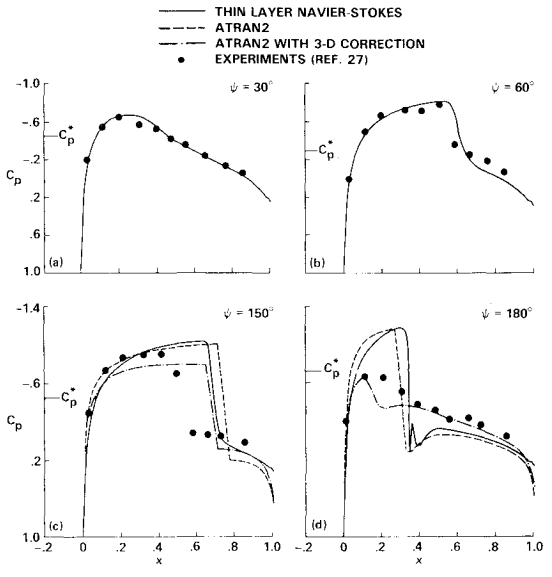

Fig. 9 Instantaneous surface-pressure distributions for the rotor-alone case: $M_T = 0.8$, $\mu = 0.2$, $r_B = 0.893$.

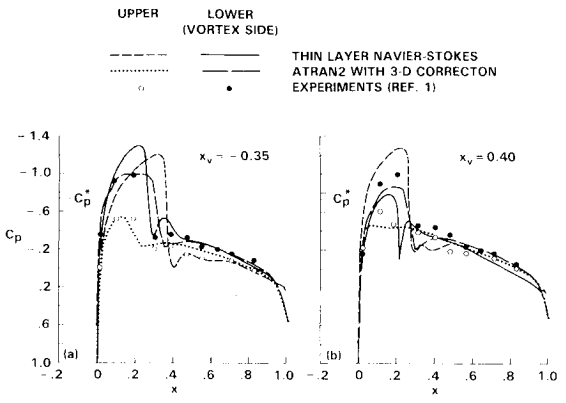

Fig. 10 Instantaneous surface-pressure distributions for the case of blade-vortex interaction: $M_T = 0.8$, $\mu = 0.2$, $\hat{\Gamma} = 0.31$, and $y_v = -0.4$.

persistence of a strong shock wave even at the $\psi = 180$ deg azimuth position, see Fig. 9d. This strongly suggests the presence of possible three-dimensional effects in addition to the unsteady shock-wave lag effects. An attempt is made to examine this aspect using transonic small-disturbance equations as described in the following paragraph.

Some ad-hoc insights into possible three-dimensional influences can be obtained from the transonic small-disturbance equation for a thin, high-aspect-ratio rotating blade,[21,22]

$$A\Phi_{tt} + B\Phi_{xt} = \frac{\partial}{\partial x}\left[C_1\Phi_x + C_2\Phi_x^2\right] + \Phi_{yy} + D\Phi_{xz} + E\Phi_{zz} \tag{10}$$

where Φ is the perturbation potential, z the spanwise coordinate, A, B, C_1, and C_2 are constants that depend on M_r and the airfoil thickness ratio, and

$$D = -2M_r\epsilon\mu'\cos\Omega t\left(z + \mu'\sin\Omega t\right)/\delta^{\frac{2}{3}}$$

$$E = \epsilon^2/\delta^{\frac{2}{3}}$$

Equation (10) reveals by inspection that three-dimensional effects influence the solution through the two terms, $D\Phi_{xz}$ and $E\Phi_{zz}$. The coefficient E is independent of Mach number, and the term $E\Phi_{zz}$ is undoubtedly important in the immediate vicinity of the tip of the rotor blade. On the other hand, the coefficient D is clearly dependent upon Mach number, as well as the blade aspect ratio, the azimuth of the rotor blade, the spanwise station along the blade, and the local advance ratio, $\mu' = U_\infty/\Omega r_B$, of the rotor. Therefore, it seems likely that this term might play the dominant three-dimensional role inboard of the tip, especially under transonic conditions.

A qualitative estimate of the influence of this cross-flow term was deduced from two-dimensional calculations in which $D\Phi_{xz}$ was added as an inhomogeneous "source" term to the basic small-disturbance code ATRAN2.[28] Namely, separation of variables, $\Phi(x, y, z, t) = F(z)\phi(x, y, t)$, was assumed, $D\Phi_{xz}$ was evaluated by assigning arbitrary constants to the ratio F'/F at a fixed $z = r_B$, and $\mathrm{d}\phi/\mathrm{d}x$ was evaluated at the previous time step. It was found that negative values of F'/F tended to strengthen the shock wave for 0 deg $< \psi <$ 90 deg and to weaken it for 90 deg $< \psi <$ 180 deg, while positive values of F'/F had the opposite effect. For example, Figs. 9c and 9d show that the small-disturbance calculations with $F'(z)/F(z) = -0.2$ approximately mimic the experimentally observed weakening of the shock wave for 150 deg $< \psi <$ 180 deg, whereas both two-dimensional results are seriously in error, by overpredicting the effects, for this supercritical case. On the other hand, results for the subcritical case depicted in Fig. 7 were found to be completely insensitive to similar (corrections due this source term) estimates of $D\Phi_{xz}$.

It must be emphasized that this reasoning is only intended to illuminate the relative importance of cross-flow effects in sub- and supercritical flows, and not to predict such effects accurately. However, this leads us to suggest that the supercritical cases of Ref. 1, with or without the vortex, are neither quasi-two-dimensional nor quasisteady. This stands in sharp contrast to the previous subcritical cases, Figs. 7 and 8, where the two-dimensional calculations are in excellent agreement with the model rotor data, and for which the only significant unsteady effects are solely a result of the airfoil-vortex interaction.

Vortex Interaction with a Rotor Blade Section

A previous attempt[9] to compute the blade-vortex interaction flowfield for the supercritical case without considering the unsteady time-lag effects produced unsatisfactory results in terms of the agreement with experiments. Such a disagreement is not surprising in view of the strong time lags and three-dimensional effects present at this supercritical condition. Figure 10 shows the results of the present calculations, including the unsteady time-lag effects, for two x locations of the vortex position during the interaction. The numerical results are calculated from both the two-dimensional, thin-layer Navier-Stokes and the modified (with the three-dimensional correction factor) transonic small-disturbance codes and are compared with the experimental data of Caradonna et al.[1] As before, the two-dimensional results overpredict the interaction effects. However, the ad-hoc three-dimensional correction to the transonic small-disturbance code (ATRAN2) seems to produce results that are in good qualitative agreement with the experiment. It should be noted that, even for this supercritical flow condition, the flow on the experimental rotor blade is subcritical (with zero lift) in the absence of the vortex interaction for the azimuth position $\psi = 180$ deg (see Fig. 9). The interacting vortex modifies the flowfield to be supercritical with strong shock waves as the interaction effects peak. As the vortex passes downstream of the blade, these supercritical conditions progressively change to subcritical conditions. Also, due to the vortex interaction, the blade develops lift which is initially negative (because of the sense of rotation of the vortex), becoming positive as the vortex passes downstream of the blade. In view of the strong viscous interaction nature of this problem, it is not surprising to see less than perfect agreement of the experiments with the approximate calculations of the transonic small-disturbance code, as shown in

Fig. 10. The purpose was only to demonstrate the existence of three-dimensional influence at the supercritical flow conditions.

Concluding Remarks

This paper presents a computational procedure to calculate the interaction flowfield of a passing vortex with a helicopter rotor blade in forward flight and numerical results for subsonic and transonic flow conditions. The interaction of the vortex considered here is one of the limiting cases of a more complex interaction typically encountered on a helicopter rotor blade and corresponds to the parallel blade-vortex interaction experimental conditions of Caradonna et al.[1] In this limit, the interaction flowfield had been previously thought to be two-dimensional and unsteady.

The present numerical scheme involves the solution of unsteady, two-dimensional, thin-layer Navier-Stokes equations implicitly using the perturbation or the prescribed-vortex approach presented in Refs. 7–9. The computational procedure is very general and accepts any arbitrary size and shape of the interacting vortex, although the structure of the vortex is assumed to remain unaltered by the interaction. From comparison of the present numerical results with the experiments, it was found that the details of the vortex structure were important.

Two test cases, a subsonic and a transonic condition corresponding to the experimental data, were chosen for the calculations. The respective blade tip Mach numbers were 0.6 and 0.8, and the blade advance ratio was 0.2. A comparison of the numerical results for these two conditions showed a very distinct difference in the flowfields, even in the absence of the interacting vortex.

The results show that, for the subcritical case, the unsteady time-lag effects are negligible for the rotating blade in the absence of the vortex, and that the unsteady flowfield with the vortex interaction is in very good qualitative and quantitative agreement with experiments. However, the supercritical case is totally dominated by strong (transonic) shock waves, the consequence of which is the presence of strong unsteady time-lag effects even in the absence of the vortex interaction. In addition, there are strong indications of the influence of three-dimensional effects. The experimental data for the rotor-alone case show the collapse of the shock wave between azimuth positions of 150 and 180 deg. The numerical results, on the other hand, show the persistence of a strong shock wave even at the 180 deg azimuth position and, thus, overpredict the experimental data.

Finally, the possibility of three-dimensional effects in the experiment, which was originally thought to be quasi-two-dimensional, was examined further using transonic small-disturbance equations with an ad-hoc three-dimensional correction. The results suggest that the three-dimensional and unsteady time-lag effects are of comparable importance, that both are negligible in purely subcritical flow, and that neither can be ignored when shock waves are present.

Acknowledgments

The research of the first author was partially supported by the U.S. Army Research Office Contract DAAG29-85-C-0002. The authors would like to express their sincere thanks to Dr. J. L. Steger for some stimulating discussions.

References

[1]Caradonna, F.X., Laub, G.H., and Tung, C., "An Experimental Investigation of the Parallel Blade-Vortex Interaction," Paper 4, Tenth European Rotorcraft Forum, The Hague, the Netherlands, Aug. 1984.

[2]McAlister, K.W. and Tung, C., "Airfoil Interaction with an Impinging Vortex," NASA TP-2273, 1984.

[3]Meier, G.E.A. and Timm, R., "Unsteady Vortex Airfoil Interaction," Paper 16, AGARD CP-386, AGARD Symposium on Unsteady Aerodynamics: Fundamentals and Applications to Aircraft Dynamics, May 1985.

[4]Padakannaya, R., "Experimental Study of Rotor Unsteady Airloads due to Blade-Vortex Interaction," NASA CR-1907, 1971.

[5]Caradonna, F.X., Tung, C., and Desopper, A., "Finite-Difference Modeling of Rotor Flows Including Wake Effects," *Journal of the American Helicopter Society*, Vol. 29, No. 2, April 1984, pp. 26-33.

[6]George, A.R. and Chang, S.B., "Noise due to Transonic Blade-Vortex Interactions," Paper A-83-39-50-D000, 39th Annual National Forum of the American Helicopter Society, May 1983.

[7]Srinivasan, G.R., McCroskey, W.J., and Kutler, P., "Numerical Simulation of the Interaction of a Vortex with a Stationary Airfoil in Transonic Flow," AIAA Paper 84-0254, Jan. 1984.

[8]McCroskey, W.J. and Srinivasan, G.R., "Transonic Interaction of Unsteady Vortical Flows," Paper 5-1, Third Symposium of Numerical and Physical Aspects of Aerodynamic Flows, Long Beach, CA, Jan. 1985; also, NASA TM-86658, 1984.

[9]Srinivasan, G.R., "Computations of Two-Dimensional Airfoil-Vortex Interactions," NASA CR-3885, 1985.

[10]Wu, J.C., Sankar, N.L., and Hsu, T.M., "Unsteady Aerodynamics of an Airfoil Encountering a Passing Vortex," AIAA Paper 85-0203, Jan. 1985.

[11]Jones, H.E., "The Aerodynamic Interaction Between an Airfoil and a Vortex in Transonic Flow," Paper presented at the Workshop on Blade-Vortex Interactions (unpublished), NASA Ames Research Center, Moffett Field, CA, Oct. 1984.

[12]Caradonna, F.X. and Philippe, J-J., "The Flow over a Helicopter Blade Tip in the Transonic Regime," *Vertica*, Vol. 2, No. 1, 1978, pp. 43-60.

[13]Beam, R.M. and Warming, R.F., "An Implicit Finite-Difference Algorithm for Hyperbolic Systems in Conservation-Law Form," *Journal of Computational Physics*, Vol. 22, Sept. 1976, pp. 87-109.

[14]Pulliam, T.H., Jespersen, D.C., and Childs, R.E., "An Enhanced Version of an Implicit Code for the Euler Equations," AIAA Paper 83-0344, 1983.

[15]Nakahashi, K. and Deiwert, G.S., "A Practical Adaptive-Grid Method for Complex Fluid-Flow Problems," *Lecture Notes in Physics*, Vol. 218, Springer-Verlag, 1984, pp. 422-426; also, NASA TM-85989, 1984.

[16]Nakahashi, K. and Deiwert, G.S., "A Self-Adaptive-Grid Method with Application to Airfoil Flow," AIAA Paper 85-1525-CP, 1985.

[17]Buning, P.G. and Steger, J.L., "Solution of the Two-Dimensional Euler Equations with Generalized Coordinate Transformation Using Flux Vector Splitting," AIAA Paper 82-0971, June 1982.

[18]Srinivasan, G.R., Chyu, W.J., and Steger, J.L., "Computation of Simple Three-Dimensional Wing Vortex Interaction in Transonic Flow," AIAA Paper 81-1206, June 1981.

[19]Steger, J.L., "Implicit Finite-Difference Simulation of Flow about Arbitrary Two-Dimensional Geometries," *AIAA Journal*, Vol. 16, July 1978, pp. 679-686.

[20]Baldwin, B.S. and Lomax, H., "Thin Layer Approximation and Algebraic Model for Separated Turbulent Flows," AIAA Paper 78-257, Jan. 1978.

[21]Isom, M.P., "Unsteady Subsonic and Transonic Potential Flow over Helicopter Rotor Blades," NASA CR-2463, 1974.

[22]Caradonna, F.X. and Isom, M.P., "Numerical Calculation of Unsteady Transonic Potential Flow over Helicopter Rotor Blades," *AIAA Journal*, Vol. 14, April 1976, pp. 482-488.

[23]Pulliam, T.H. and Steger, J.L., "On Implicit Finite-Difference Simulations of Three-Dimensional Flow," *AIAA Journal*, Vol. 18, Feb. 1980, pp. 159-167.

[24]Srinivasan, G.R. and McCroskey, W.J., "Computations of Blade-Vortex Interaction by Different Methods," Paper presented at the Workshop on Blade-Vortex Interactions (unpublished), NASA Ames Research Center, Moffett Field, CA, Oct. 1984.

[25]Takahashi, R.K. and McAlister, K.W., "Preliminary Measurements of a Wing-Tip Vortex Using Laser Velocimetry," U.S. Army Aeroflightdynamics Directorate, NASA Ames Research Center, Moffett Field, CA, 1985, personal communication.

[26]Orloff, K.L. and Grant, G.R., "The Application of Laser Doppler Velocimetry to Trailing Vortex Definition and Alleviation," NASA TM X-62,243, 1973.

[27]Tung, C., U.S. Army Aeroflightdynamics Directorate, NASA Ames Research Center, Moffett Field, CA, 1985, personal communication.

[28]McCroskey, W. J. and Goorjian, P. M., "Interactions of Airfoils with Gusts and Concentrated Vortices in Unsteady Transonic Flow," AIAA Paper 83-1691, July 1983.